



## OPEN PRSS22 as a novel prognostic and immune regulatory biomarker in PanCancer multiomics analysis

Tao Jiang<sup>1,2</sup>, Jialin Liu<sup>1,4</sup>, Hao Chen<sup>1,2,4</sup>, Fangyu Lin<sup>1,2</sup>, Xiaojiao Weng<sup>1,2</sup>, Qing Liu<sup>1,2</sup>, Han Wang<sup>1,2</sup>, Bin Du<sup>1,2</sup>, Xinli Wang<sup>1,2</sup>, Xiaoyan Lin<sup>1,2</sup> & Wenyu Gao<sup>3✉</sup>

Serine proteases are key mediators of tumorigenesis; however, the pan-cancer significance of PRSS22 remains poorly defined. This study comprehensively analyzes the multi-omics landscape and clinical relevance of PRSS22 across 33 cancer types using data from TCGA, HPA, and cBioPortal. We performed systematic analyses, including expression profiling (cancer vs. normal), prognosis (overall survival), characterization of the immune microenvironment, functional enrichment, and assessment of genomic alterations. PRSS22 expression demonstrated significant cancer-type specificity, with frequent overexpression observed in 10 cancer types and downregulation in 4 cancer types ( $p < 0.05$ ). Notably, elevated tumor expression levels of PRSS22 were independently associated with worse overall survival in multiple cancers, specifically KIRC, LIHC, LUAD, and SKCM ( $p < 0.05$ ). Despite showing downregulation at the mRNA level in KIRC, LIHC, and SKCM cancer cell lines as validated by qPCR, higher tumor tissue PRSS22 expression in patient cohorts of these cancers remained strongly associated with poor prognosis—a paradox suggesting potential non-cell-autonomous roles. Furthermore, PRSS22 levels showed associations with the tumor immune microenvironment. Functional enrichment analyses indicated that PRSS22 co-expressed/related genes are enriched in diverse biological processes relevant to cancer. Our pan-cancer analysis establishes PRSS22 as a multifaceted biomarker with prognostic value and links to tumor immunity, highlighting its complex, context-dependent roles across malignancies. These findings provide a crucial foundation for elucidating PRSS22's mechanisms and assessing its potential for diagnostic/prognostic applications.

**Keywords** PRSS22, Pan-Cancer analysis, Tumor immune microenvironment, Multi-omics, Serine protease

Cancer remains a leading cause of global mortality, with tumor heterogeneity and dysregulated molecular pathways posing significant challenges<sup>1</sup>. Serine proteases, a class of enzymes involved in extracellular matrix remodeling, immune modulation, and cellular signaling, have emerged as critical regulators of oncogenesis and tumor progression<sup>2,3</sup>. The PRSS22 gene, mapping to chromosome 16p13.3, was initially identified as a member of the serine protease family. It is primarily expressed in airway epithelial cells under physiological conditions and is involved in extracellular matrix remodeling, immune regulation, and cellular signaling<sup>4,5</sup>. Among these, PRSS22 has been implicated in tumorigenesis through its potential roles in proteolytic cascades and microenvironmental interactions<sup>6</sup>. However, a comprehensive pan-cancer analysis of PRSS22—incorporating its expression patterns, prognostic significance, and mechanistic connections with immune infiltration—has not been thoroughly investigated, thus constraining its potential clinical application as a biomarker or therapeutic target.

Recent advances in multi-omics databases, including The Cancer Genome Atlas (TCGA)<sup>7</sup> and the Human Protein Atlas (HPA)<sup>8</sup>, provide unprecedented opportunities to decode cancer-associated genes across diverse malignancies. While preliminary studies have linked PRSS22 to specific cancers<sup>6,9</sup>, its pan-cancer expression profile, mutation landscape, and interactions with tumor-infiltrating immune cells remain poorly characterized. Furthermore, conflicting reports on the tissue-specific roles underscore the need for systematic investigations that integrate genomic, proteomic, and clinical datasets<sup>10</sup>.

<sup>1</sup>Department of Medical Oncology, Fujian Medical University Union Hospital, Fuzhou 350001, People's Republic of China. <sup>2</sup>Fujian Provincial Key Laboratory of Translational Cancer Medicine, Fuzhou 350001, People's Republic of China. <sup>3</sup>Department of Gastroenterology, Fujian Medical University Union Hospital, 29 Xinquan Road, Fuzhou 350001, Fujian, People's Republic of China. <sup>4</sup>Jialin Liu and Hao Chen contributed equally to this work. ✉email: 13696951525@163.com

This study aims to provide a comprehensive pan-cancer evaluation of PRSS22, integrating multi-omics data. We systematically analyzed transcriptomes from TCGA/GTEX and protein expression from HPA, then performed experimental validation using quantitative real-time PCR (qPCR) to characterize PRSS22 expression patterns and assess its prognostic relevance. Functional enrichment and protein–protein interaction (PPI) network analyses were employed to identify associated biological pathways. Further investigations into its relationship with tumor immunity and genomic instability were undertaken using immune deconvolution methods and mutation burden analysis. Collectively, this work aims to evaluate PRSS22 as a candidate multi-faceted biomarker for prognostication and immunotherapy stratification, with computational insights guiding future mechanistic and clinical studies.

## Materials and methods

### Data acquisition and processing

Transcriptomic and clinicopathological data for 33 cancer types were obtained from public databases, with detailed acquisition and processing procedures as follows: RNA sequencing (RNAseq) data of 33 cancer projects processed by the STAR workflow were downloaded and curated from the TCGA Data Portal (<https://portal.gdc.cancer.gov/>), from which transcriptomic data in Transcripts Per Million (TPM) format were extracted. Additionally, RNAseq data in TPM format—uniformly processed using the Toil workflow<sup>11</sup>—were retrieved from the UCSC XENA platform (<https://xenabrowser.net/datapages/>), which integrates transcriptomic data from both TCGA (corresponding to the 33 pan-cancer types mentioned above) and the Genotype-Tissue Expression (GTEx) project. Genes significantly co-expressed with PRSS22 (top 100, Pearson correlation  $p < 0.05$ ) were identified using Gene Expression Profiling Interactive Analysis 2 (GEPIA2) (<http://gepia2.cancer-pku.cn/>)<sup>12</sup>. The three-dimensional (3D) structure of the PRSS22 protein was predicted using the AlphaFold Protein Structure Database (<https://alphafold.ebi.ac.uk/>)<sup>13</sup>, with per-residue confidence scores (pLDDT) indicating reliability. This study complied with TCGA data usage guidelines for de-identified public datasets, which waive additional ethical approval.

### Pan-cancer expression profiling

PRSS22 expression was evaluated across: (1) TCGA tumors ( $n = 11,123$ ), (2) combined TCGA tumors and GTEx normal tissues ( $n = 18,102$ ), (3) TCGA-matched tumor-normal pairs ( $n = 1404$ ). Normalization used  $\log_2(\text{TPM} + 1)$ -transformed counts. Differential expression required  $|\log_2 \text{fold change}| > 1$  (FDR-adjusted  $q < 0.05$ , Benjamini–Hochberg method). Immunohistochemical (IHC) profiles of PRSS22 in normal and neoplastic tissues were obtained from the HPA (<https://www.proteinatlas.org/>) for visual reference.

### qPCR validation of PRSS22 expression

Normal control and cancer cell lines representing four tumor types were cultured in appropriate media: (1) Kidney Renal Clear Cell Carcinoma (KIRC): HK2 (control), 786-O, A498, SW839. (2) Liver Hepatocellular Carcinoma (LIHC): LX-2 (control), Huh-7, JHH-7, HCCLM3. (3) Lung Adenocarcinoma (LUAD): BEAS-2B (control), A549, H1299, HCC827. (4) Skin Cutaneous Melanoma (SKCM): HaCaT (control), A375, A2058, SK-MEL-28. Following standard protocols, total RNA was extracted, reverse transcribed into cDNA, and subjected to qPCR using PRSS22-specific primers: forward: 5'-TGTCTCGGCACCTTCACCT-3', reverse: 5'-GAATACA CAGGGTGGGGCTC-3'. Gene expression was normalized to GAPDH and quantified via the  $2^{-\Delta\Delta C_t}$  method. Detailed experimental protocols are provided in Supplementary Material 1.

### Prognostic and clinicopathological correlation analysis

Cox proportional hazards regression was used to evaluate the association between PRSS22 expression and overall survival (OS) across 33 malignancies<sup>14</sup>. Survival curves were generated for cancers with significant hazard ratios ( $p < 0.05$ ). Clinicopathological parameters (gender, T/N/M stage, pathological stage, etc.) were analyzed using the Wilcoxon rank-sum and Kruskal–Wallis tests. The diagnostic efficacy in prognosis-linked cancers was assessed using receiver operating characteristic (ROC) curves.

### Nomogram development

Cancer types with significant univariate Cox associations ( $p < 0.05$ ) and sample size  $> 400$  were included. Multivariable Cox models incorporated PRSS22 expression, TNM stage, pathological stage, and serum biomarkers, among others. Nomograms were built using survival (v3.3-1) and rms (v6.3-0) in R. Calibration curves validated 1-, 3-, and 5-year OS predictions.

### PRSS22-associated cell clustering and classification

Download the corresponding single-cell data in .h5 format and annotation results from TISCH2 (<http://tisch.cmp-genomics.org/>)<sup>15</sup>. Process and analyze the single-cell data using the R software packages MAESTRO (v1.8.0) and Seurat (v4.1.0). Then, cell clustering and grouping will be performed using the t-SNE method.

### Protein–protein interaction (PPI) network

The STRING database (<https://string-db.org/>; confidence score  $> 0.15$ ) was queried to identify PRSS22-interacting proteins<sup>16</sup>. The PPI network was visualized and topologically analyzed (using degree centrality and betweenness) with Cytoscape (v3.9.1), with functional modules annotated via the MCODE plugin.

### Immune infiltration analysis

PRSS22's correlation with immune cell abundance (such as B cells, macrophages, CD4+/CD8+ T cells) was assessed using TIMER2.0 (<http://timer.cistrome.org/>)<sup>17</sup> and CIBERSORT algorithms<sup>18</sup>. Immune cell fraction

distributions were visualized as stacked bar plots<sup>19</sup>. Immune infiltration analysis was performed using the ssGSEA algorithm provided by the R package GSVA [1.46.0], which utilizes markers for 24 immune cell types to calculate the immune infiltration status<sup>20</sup>. The lollipop chart was generated using the ggplot2 package, displaying the correlation coefficients and their statistical significance. The scatter plot, also created with the ggplot2 package, visually represents the relationship between PRSS22 expression levels and the extent of specific immune cell infiltration. The correlation between PRSS22 and immune activation, as well as exhaustion markers<sup>21</sup> was analyzed using the GEPIA2 online platform with Spearman's rank correlation coefficient.

### Functional enrichment analysis

GEPIA2-derived PRSS22-correlated genes (top 100) underwent Gene Ontology (GO: BP/CC/MF) and KEGG pathway analysis<sup>22–24</sup> via the clusterProfiler R package (v4.4.4)<sup>25</sup>. Differential expression genes (DEGs) in prognostic cancers were identified using DESeq2 (FDR < 0.05), followed by gene set enrichment analysis (GSEA) for pathway annotation<sup>26</sup>.

### Genomic alteration profiling

Mutation frequencies, copy number variations (CNAs), and mRNA alterations of PRSS22 were analyzed via cBioPortal (<https://www.cbioportal.org/>)<sup>27</sup> using TCGA pan-cancer datasets.

### Statistical analysis

Bioinformatic analyses were conducted using the Xiantao platform (<https://www.xiantao.love/products>), which operates within the R statistical computing environment. Group comparisons were performed using the Wilcoxon test (for two groups) or the Kruskal–Wallis test (for three or more groups). Spearman's rank evaluated correlations. qPCR data from three biological replicates were analyzed by one-way ANOVA with Tukey's post-hoc test (GraphPad Prism v9.4.0; results: mean ± SD; \*  $p < 0.05$ , \*\*  $p < 0.01$ , \*\*\*  $p < 0.001$ ).

## Results

### Dysregulated PRSS22 expression in pan-cancer and predicted 3D structure

Integrated analysis of TCGA\_GTEX and TCGA datasets revealed tumor-specific dysregulation of PRSS22: significant upregulation ( $\log_2FC > 1$ ,  $p < 0.05$ ) was observed in 10 cancer types, such as Bladder Urothelial Carcinoma (BLCA) and LUAD, while downregulation was identified in 4 cancers, including Kidney Chromophobe (KICH) (Fig. 1A–C). AlphaFold generated a predicted 3D structure of the PRSS22 protein, revealing its folding patterns and functional regions (Fig. 1D). HPA IHC images indicated elevated PRSS22 protein expression in BLCA and LUAD tumors relative to adjacent normal tissues. In contrast, Breast Cancer (BRCA) exhibited comparable expression levels (Fig. 1E).

### Experimental validation of PRSS22 expression via qPCR

To empirically validate the dysregulated PRSS22 expression patterns identified in our pan-cancer analysis, we performed qPCR assays on cell lines representing four malignancies: KIRC, LIHC, LUAD, and SKCM. Using established normal cell lines as controls (HK2 for KIRC, LX-2 for LIHC, BEAS-2B for LUAD, and HaCaT for SKCM), we assessed PRSS22 mRNA levels in triplicate experiments. In line with the bioinformatic results, PRSS22 expression showed notable cancer-specific changes. Specifically, in KIRC models, PRSS22 was markedly downregulated in 786-O, A498, and SW839 cells compared to HK2 controls ( $p < 0.01$ ) (Fig. 2A). Similarly, LIHC cell lines (Huh-7, JHH-7, HCCLM3) showed reduced expression relative to LX-2 ( $p < 0.01$ ) (Fig. 2B). Conversely, LUAD-associated cells (A549, H1299, HCC827) demonstrated pronounced upregulation versus BEAS-2B ( $p < 0.05$ ) (Fig. 2C). In SKCM, A375, A2058, and SK-MEL-28 cells exhibited suppressed PRSS22 levels compared to HaCaT ( $p < 0.01$ ) (Fig. 2D).

### Prognostic significance of PRSS22

The forest plot (Fig. 3A) presents the univariate Cox analysis results of the PRSS22 gene across multiple tumors, including the  $p$ -value, hazard ratio (HR), confidence interval of HR,  $\beta$  value, Wald value, and standard error (SE). Cox regression identified PRSS22 as an independent prognostic marker in KIRC ( $p = 0.015$ , HR 1.45, 95% CI 1.07–1.96), LIHC ( $p = 0.027$ , HR 1.50, 1.05–2.16), LUAD ( $p = 0.017$ , HR 1.42, 1.06–1.89), and SKCM ( $p = 0.044$ , HR 1.32, 1.01–1.73; Fig. 3B)—high PRSS22 expression correlated with reduced OS. ROC curves demonstrated favorable diagnostic performance across prognostic-linked cancers, with AUC values ranging from 0.793 to 0.957 (95% CI shown in Fig. 3C), supporting its potential clinical utility.

### Clinicopathological associations

In KIRC, PRSS22 levels positively correlated with Race ( $p < 0.001$ ) and Serum calcium ( $p < 0.01$ ) (Fig. S1A). LIHC exhibited associations with AFP, Age, and Residual tumor ( $p < 0.05$ ) (Fig. S1B). SKCM showed linkages to Breslow depth ( $p < 0.001$ ), Melanoma ulceration ( $p < 0.01$ ), Melanoma Clark level, Pathologic T stage, and Tumor tissue site ( $p < 0.05$ ) (Fig. S1C), while LUAD correlated with Anatomic neoplasm subdivision ( $p < 0.05$ ) (Fig. S1D).

### Nomogram predictive performance

Multivariable Cox models were constructed to integrate PRSS22 expression with clinicopathological factors for KIRC, LIHC, LUAD, and SKCM. The models yielded C-indices of 0.575 (KIRC), 0.584 (LIHC), 0.544 (LUAD), and 0.655 (SKCM), indicating modest predictive accuracy. Calibration curves for 1-, 3-, and 5-year survival probabilities are provided in Fig. S1E.

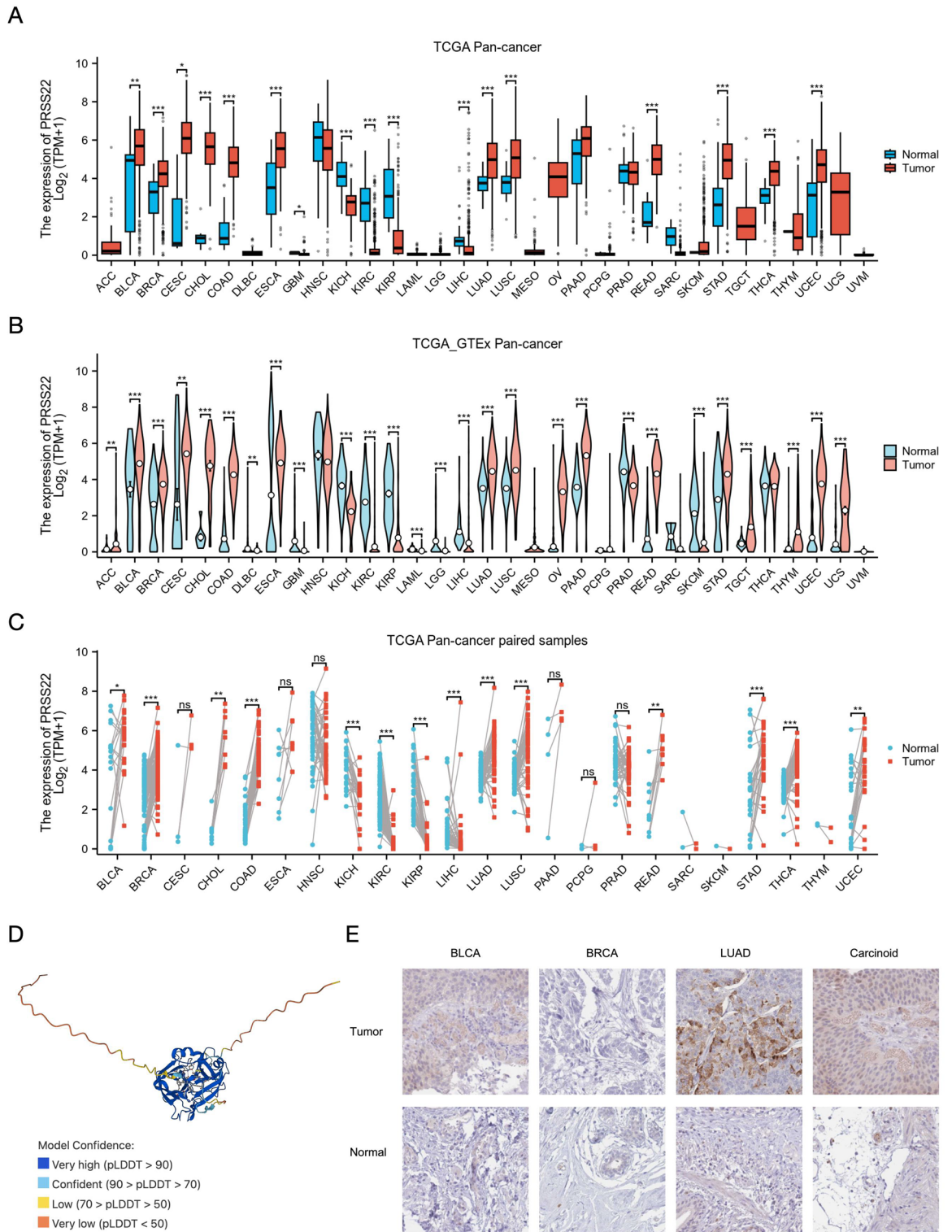


**Fig. 1.** Expression patterns and predicted structure of PRSS22 in human cancers. **(A)** The expression of PRSS22 mRNA across 33 types of tumors was analyzed in the TCGA databases. **(B)** The expression of PRSS22 mRNA across 33 types of tumors in TCGA\_GTEX. **(C)** PRSS22 expression in paired tumor-normal samples from 23 TCGA cohorts. **(D)** Predicted 3D structure of PRSS22 by AlphaFold, with pLDDT confidence scores. **(E)** Protein expression of PRSS22 in tumor and normal tissues. (ns,  $p > 0.05$ ; \* $p < 0.05$ ; \*\* $p < 0.01$ ; \*\*\* $p < 0.001$ ).

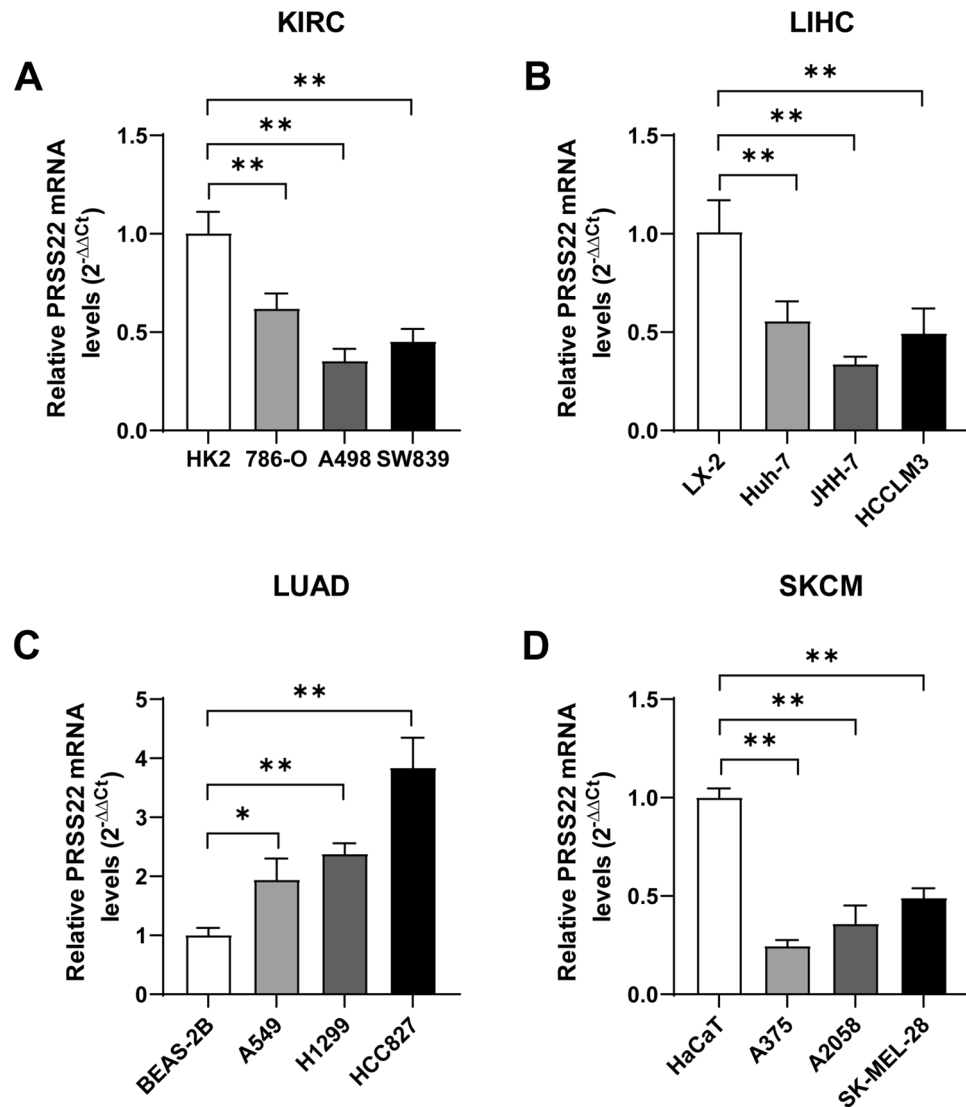


**Fig. 2.** Differential gene expression of PRSS22 in cancer cells. **(A)** KIRC: PRSS22 mRNA was significantly downregulated in 786-O, A498, and SW839 cell lines compared to the human renal proximal tubule epithelial cell line HK2 ( $p < 0.01$ ). Expression ranking: HK2 > 786-O > SW839 > A498. **(B)** LIHC: PRSS22 showed marked downregulation in Huh-7, JHH-7, and HCCLM3 cells relative to the hepatic stellate cell line LX-2 ( $p < 0.01$ ). Expression ranking: LX-2 > Huh-7 > HCCLM3 > JHH-7. **(C)** LUAD: PRSS22 was significantly upregulated in A549, H1299, and HCC827 cells compared to the normal bronchial epithelial cell line BEAS-2B ( $p < 0.05$ ). Expression ranking: HCC827 > H1299 > A549 > BEAS-2B. **(D)** SKCM: Pronounced downregulation was observed in A375, A2058, and SK-MEL-28 melanoma cells versus the immortalized human keratinocyte line HaCaT ( $p < 0.01$ ). Expression ranking: HaCaT > SK-MEL-28 > A2058 > A375. \* $p < 0.05$ , \*\* $p < 0.01$ .

### Cluster analysis and classification of cells related to PRSS22

The single-cell clustering analysis revealed distinct cell clustering patterns associated with PRSS22 across the different cancer types. In KIRC (GSE145281), NSCLC (GSE179373), and SKCM (GSE139249), we observed notable clusters of CD4+ and CD8+ T cells. In contrast, the LIHC dataset (GSE146409) predominantly clustered epithelial cells (Fig. 4A–C).

### Protein–protein interaction network topology

To explore the functional implications and interaction networks of PRSS22, PPI data were retrieved from the STRING database using a confidence threshold > 0.15. The interaction network was reconstructed and visualized using Cytoscape (v3.9.1), revealing PRSS22 as a central hub interconnected with multiple binding partners (Fig. 5A).

### Association of PRSS22 with immune cell infiltration and immune markers

To comprehensively evaluate the role of PRSS22 in tumor immunomodulation, we analyzed its relationship with immune cell infiltration and key immune markers across various malignancies using TCGA data via TIMER 2.0.

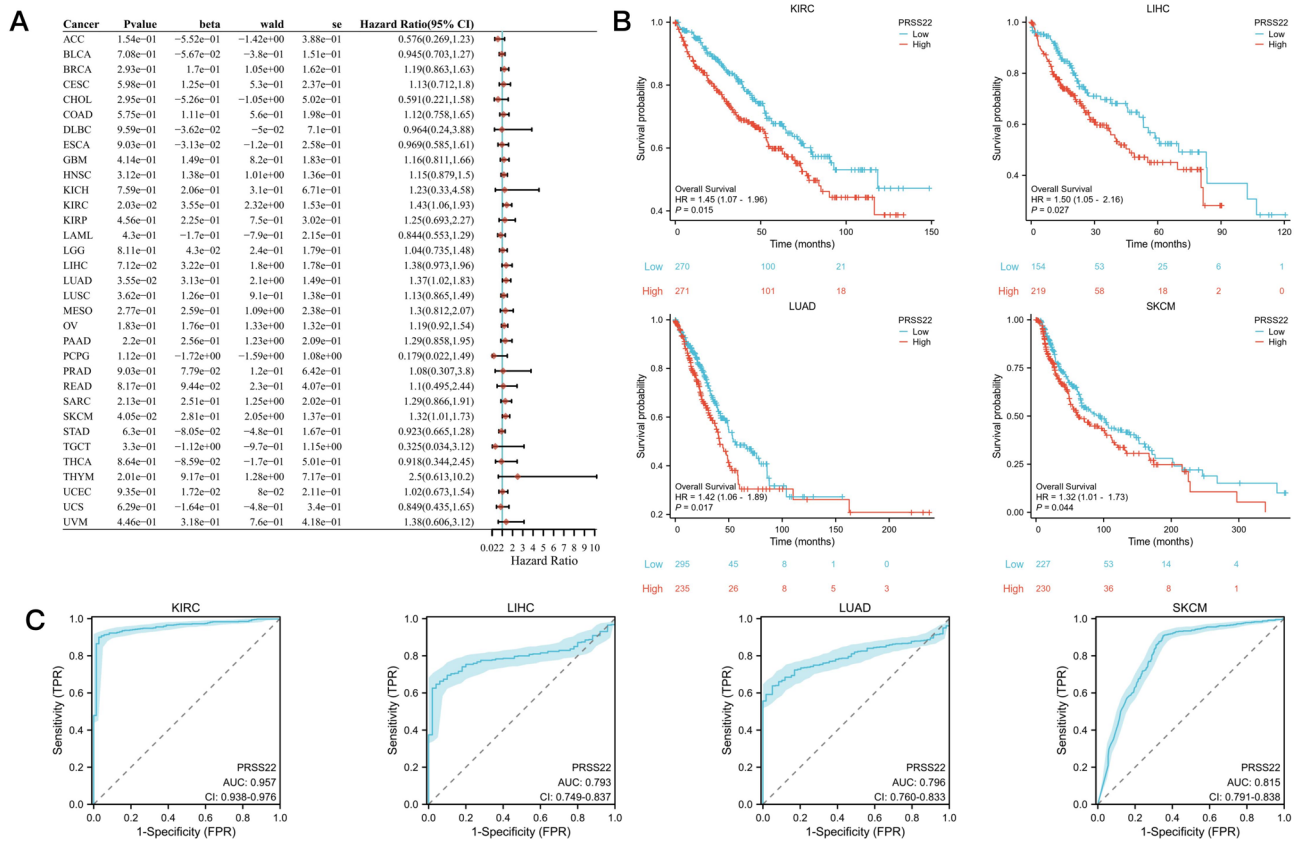


**Fig. 3.** Prognostic and diagnostic value of PRSS22 expression across cancers. **(A)** Forest plot depicting the association between PRSS22 expression and OS in a pan-cancer analysis (Cox proportional hazards model) **(B)** Kaplan–Meier survival curves showing the impact of high versus low PRSS22 expression on OS in four representative cancers: KIRC, LIHC, LUAD, and SKCM. **(C)** Diagnostic efficacy of PRSS22 expression in prognosis-linked cancers assessed via ROC curves.

Heatmaps were created to depict the correlation between PRSS22 expression and B cells, macrophages, CD4+ T cells, and CD8+ T cells (Fig. 5B) in a pan-cancer context. Furthermore, stacked bar plots depicting PRSS22-associated immune cell fractions were constructed for KIRC, LIHC, LUAD, and SKCM, providing a comparative visualization of immune infiltration patterns across these malignancies (Fig. 5C).

Detailed immune infiltration analysis across four malignancies revealed distinct PRSS22-immune cell relationships: (1) KIRC: Positive correlation with NK cells activated ( $R = 0.122$ ,  $p = 0.004$ ); Negative correlation with Macrophages M2 ( $R = -0.139$ ,  $p = 0.001$ ). (2) LIHC: Positive correlation with Macrophages M0 ( $R = 0.236$ ,  $p < 0.001$ ); Negative correlation with Macrophages M1 ( $R = -0.144$ ,  $p = 0.005$ ). (3) LUAD: Positive correlation with Macrophages M0 ( $R = 0.174$ ,  $p < 0.001$ ); Negative correlation with Plasma cells ( $R = -0.160$ ,  $p < 0.001$ ). (4) SKCM: Positive correlation with Macrophages M0 ( $R = 0.220$ ,  $p < 0.001$ ); Negative correlation with T cells CD8 ( $R = -0.113$ ,  $p < 0.014$ ). These associations were visualized through lollipop charts and substantiated by scatter plots with annotated regression lines, correlation coefficients, and  $p$ -values (Fig. 5D).

Additionally, we systematically evaluated the associations between PRSS22 expression and key immune markers, including activation markers (CD28, TNFRSF9) and exhaustion markers (PDCD1, HAVCR2, CTLA4, TIGIT), across different malignancies. Applying criteria of  $|R| > 0.2$  and  $p < 0.05$ , tissue-specific correlations emerged: In KIRC, PRSS22 showed a significant negative correlation with the exhaustion marker TNFRSF9 ( $R = -0.22$ ; Fig. S2A). In LIHC, PRSS22 was strongly positively correlated with both activation markers CD28 ( $R = 0.22$ ) and TNFRSF9 ( $R = 0.24$ ), and exhaustion markers PDCD1 ( $R = 0.34$ ), HAVCR2 ( $R = 0.45$ ), CTLA4 ( $R = 0.30$ ), and TIGIT ( $R = 0.26$ ) (Fig. S2B). No significant associations were found in LUAD or SKCM (Fig. S2C–D).

### Functional enrichment insights

To elucidate the biological roles of PRSS22 in tumorigenesis, the top 100 co-expressed genes with PRSS22 were identified using the GEPIA2 database. GO enrichment analysis revealed that PRSS22-associated genes are significantly involved in diverse biological processes (BP), including, but not limited to, epidermis development, skin development, epidermal cell differentiation, and keratinocyte differentiation. Cellular component (CC) analysis highlighted associations with cell–cell junctions, desmosomes, gap junctions, and connexin complexes. At the same time, molecular function (MF) terms included cadherin binding, calcium-dependent protein

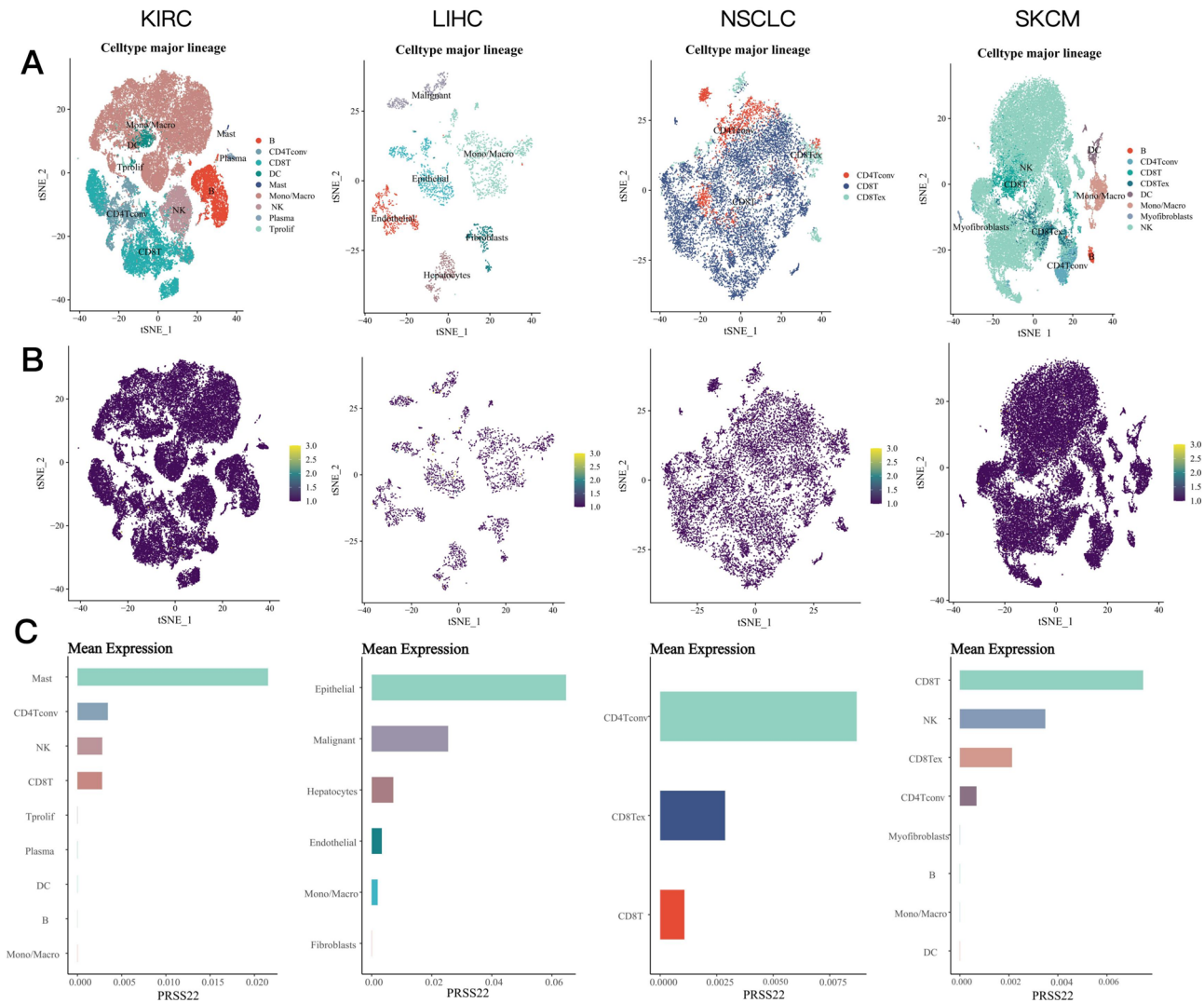


**Fig. 4.** PRSS22-associated cell clusters in KIRC (GSE145281), NSCLC (GSE179373), and SKCM (GSE139249) are linked to distinct CD4<sup>+</sup> and CD8<sup>+</sup> T cell clusters, while LIHC (GSE146409) primarily clusters epithelial cells related to PRSS22 expression. **(A)** t-SNE plots for single-cell clustering, with different colors representing various cell types. **(B)** t-SNE plots for the expression distribution of PRSS22 across different cell types, where darker colors represent lower expression and brighter colors represent higher expression. **(C)** Bar plots showing the expression abundance of PRSS22 in different cell types.

binding, and cell–cell adhesion mediator activity (Fig. 6A). To investigate PRSS22's functional significance further, GSEA was performed based on its differential expression patterns in KIRC, LIHC, LUAD, and SKCM. The results revealed associations between PRSS22 expression and key oncogenic pathways, including, but not limited to, FCGR activation, CD22-mediated BCR regulation, ECM regulators, constitutive signaling by aberrant PI3K in cancer, PD1 signaling, p53 signaling pathway, and DNA methylation (Fig. 6B).

### Genomic alteration landscape

Genomic alteration profiling of PRSS22 was performed using cBioPortal tools across multiple cancer types. The results revealed heterogeneous mutation profiles, with PRSS22 copy number amplifications most frequently observed in breast cancer. In contrast, melanoma exhibited the highest mutation frequency. Additionally, deep deletions of PRSS22 were detected in breast cancer, ovarian cancer, esophago-gastric cancer, hepatobiliary cancer, and embryonal tumors, suggesting genomic instability (Fig. 6C).

### Discussion

This pan-cancer multi-omics analysis identifies PRSS22 as a multifaceted biomarker with potential in prognostication and reveals its associations with immune landscapes across malignancies. Our findings reinforce the emerging role of serine proteases in tumorigenesis while providing a systemic, multi-omics perspective on PRSS22 functionality<sup>6,28,29</sup>.

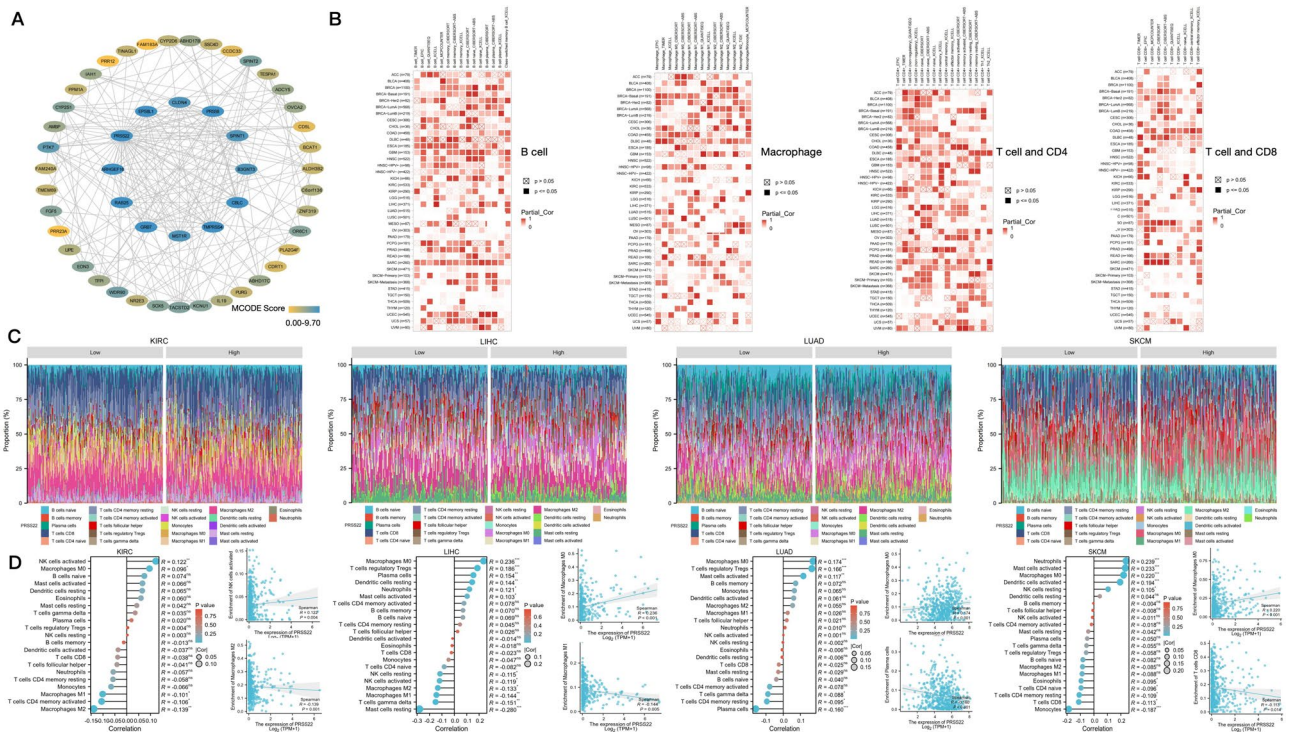


**Fig. 5.** Integrated analysis of PRSS22 protein interactions and immune infiltration patterns. **(A)** PPI network of PRSS22 and its interacting partners. **(B)** Heat maps illustrate the correlations between PRSS22 expression and immune cell types, including B cells, macrophages, CD4 + T cells, and CD8 + T cells, in the TIMER2 database, respectively. **(C)** Stacked bar plots of PRSS22-associated immune cell fractions in KIRC, LIHC, LUAD, and SKCM. **(D)** Lollipop chart and scatter plots depicting the correlation between PRSS22 expression and specific immune cell infiltration in KIRC, LIHC, LUAD, and SKCM. The lollipop chart shows correlation coefficients for various immune cell types, and scatter plots illustrate the relationship between PRSS22 and specific immune cells with regression lines, correlation coefficients, and *p*-values annotated.

The dysregulated expression of PRSS22 across various cancer types highlights its potential as a pan-cancer biomarker, warranting further investigation. We observed distinct expression patterns: PRSS22 was frequently overexpressed in malignancies such as LUAD, where elevated levels correlated with reduced OS, supporting its utility as an adverse prognostic marker. Conversely, our qPCR analysis revealed a significant downregulation of PRSS22 mRNA in cultured cell lines derived from KIRC, LIHC, and SKCM. This pattern of cancer-cell-intrinsic suppression presents an apparent paradox when contrasted with our analysis of TCGA clinical cohorts. This apparent discrepancy suggests that the source and biological impact of PRSS22 expression within the tumor microenvironment (TME) are critically important<sup>30</sup>. We propose that stromal or immune cells within the TME may overexpress PRSS22 to drive progression. Further research is needed to elucidate the exact mechanisms underlying this discrepancy and to clarify the role of PRSS22 in different tumor contexts.

The predicted structure of PRSS22, characterized by its complex folding and functional domains, offers a framework for hypothesizing its interactions with other biomolecules. This computational model provides a basis for exploring PRSS22's physiological and pathological functions. Furthermore, the application of AlphaFold exemplifies the value of advanced computational tools in structural biology, enabling efficient exploration of protein functions and informing therapeutic strategy development<sup>31</sup>. While the predicted structure informs mechanistic hypotheses, experimental validation of PRSS22's active sites remains essential to confirm its functional roles. The PPI network analysis positions PRSS22 as a highly connected node that interacts with multiple proteins, consistent with its involvement in diverse tumor-associated processes. Functional enrichment links PRSS22 to biological processes, including epidermal cell differentiation and cell-cell adhesion, suggesting its role in maintaining tissue integrity and its potential dysregulation in cancer<sup>32</sup>. As a serine protease, PRSS22's substrates warrant experimental validation. Our PPI network identified key interactors, including protease inhibitors (SPINT1, SPINT2), cell adhesion regulators (CLDN4, TACSTD2), and membrane proteases (TMPRSS4). These interactions, particularly with Kunitz-type inhibitors (SPINT1/2)<sup>33</sup>, suggest inhibitory complexes may regulate PRSS22. Functional enrichment further implicates extracellular matrix components as candidate substrates.

The cluster analysis and classification of cells related to PRSS22 across KIRC, LIHC, NSCLC, and SKCM reveal distinct cell clustering patterns associated with PRSS22 across the different cancer types. In KIRC, NSCLC, and SKCM, we observed notable clusters of CD4+ and CD8+ T cells, indicating a potential immune-related role of PRSS22 in these cancers. This is consistent with previous studies highlighting the importance of T cell subsets in the TME<sup>34,35</sup>. In the LIHC dataset, epithelial cells constituted the predominant population associated

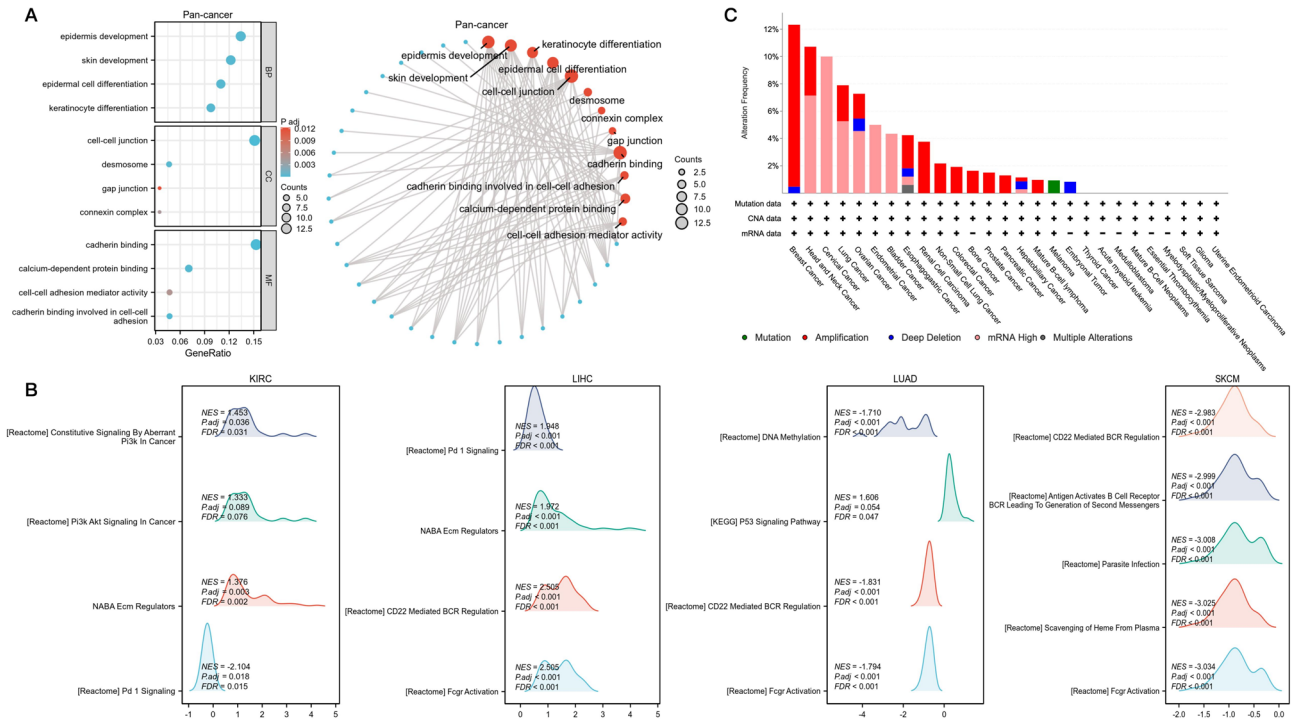


**Fig. 6.** Integrative functional and genomic profiling of PRSS22-associated pathways. **(A)** Gene Ontology (GO) enrichment of the top 100 PRSS22-correlated genes. Biological Processes (BP): epidermal morphogenesis, keratinocyte differentiation. Cellular Components (CC): cell–cell junctions, desmosome assembly. Molecular Functions (MF): cadherin binding, calcium-dependent adhesion. **(B)** Gene Set Enrichment Analysis (GSEA) of PRSS22-differential expression in KIRC, LIHC, LUAD, and SKCM RNA-seq data. Key pathways: FCGR activation, CD22-mediated BCR regulation, ECM regulators, constitutive signaling by aberrant PI3K in cancer, PD1 signaling, p53 signaling pathway, and DNA methylation. **(C)** Pan-cancer genomic alteration profile via cBioPortal. Top alterations: amplifications (breast cancer), mutations (melanoma), deep deletions (embryonal tumors, suggesting genomic instability).

with PRSS22 expression. This epithelial-centric pattern aligns with established knowledge of hepatocellular carcinoma biology, where epithelial cell dysregulation is a hallmark of disease progression<sup>36</sup>. Such context-specific expression may reflect distinct roles for PRSS22 in liver carcinogenesis compared to other malignancies.

Immune infiltration analysis revealed significant correlations between PRSS22 expression and the abundance of specific immune cell types, suggesting a potential role in modulating the tumor immune microenvironment. These associations may hold relevance for immunotherapy development, where deciphering tumor-immune interactions informs treatment strategies<sup>37</sup>. Critically, our marker correlation analysis extends these insights by revealing PRSS22’s tissue-specific coordination of T-cell dysfunction programs. In LIHC, PRSS22 concurrently correlated with both T-cell activation (CD28, TNFRSF9) and exhaustion markers (PDCD1, CTLA4, HAVCR2, TIGIT), suggesting its role in fostering an immune-tolerant niche where chronic stimulation drives T-cells toward dysfunction<sup>38</sup>. This aligns with our pathway enrichment, which shows PRSS22-linked PD-1 signaling. Conversely, in KIRC, the negative correlation trend between PRSS22 and TNFRSF9—a key enhancer of CD8 T-cell antitumor activity—indicates suppression of cytotoxic priming<sup>39</sup>. Such duality underscores PRSS22 as a contextual immune regulator: potentiating exhaustion in “hot” tumors (e.g., LIHC) while dampening activation in “cold” microenvironment (e.g., KIRC).

Functional enrichment analysis associated PRSS22 with biological processes critical for tissue integrity maintenance and regulation of cell proliferation/differentiation—key hallmarks of tumorigenesis<sup>40,41</sup>. Specifically, PRSS22-correlated genes showed enrichment in cell adhesion and communication pathways, including cell–cell junctions and desmosomes. Moreover, PRSS22 expression patterns were linked to immune regulation, ECM remodeling, PI3K signaling, DNA methylation, and p53 pathway activity<sup>42–44</sup>. The observed genomic alteration landscape—featuring frequent copy number amplifications and mutations—further aligns with PRSS22’s potential contribution to genomic instability in cancer<sup>45</sup>. Collectively, these findings position PRSS22 as a molecular nexus potentially influencing tumor development through diverse mechanisms.

This pan-cancer study establishes PRSS22 as a molecular nexus with dysregulated expression across malignancies and prognostic associations, positioning it as a compelling candidate for further investigation in tumor biology. While mechanistic insights were previously confined to specific cancers—notably the ANXA1/FPR2/ERK axis in breast cancer metastasis<sup>6</sup>—our multi-omics profiling uncovers three interconnected dimensions of PRSS22 functionality that transcend tissue boundaries: (1) Immune Microenvironment Orchestration: PRSS22 expression correlates with altered immune cell infiltration landscapes, particularly

showing positive association with CD8+T cell abundance<sup>46</sup>. This pattern suggests potential involvement in adaptive immune responses, where PRSS22 may act as a modulator of antitumor immunity through the regulation of chemokine processing or checkpoint ligand activity. (2) Oncogenic Pathway Convergence: PRSS22 engages core tumorigenic pathways including PD-1 signaling, PI3K activation, and p53 dysregulation. Such pathway pleiotropy suggests that it may function as a signaling node that amplifies oncogenic cues in a context-dependent manner, potentially explaining its variable prognostic impacts across different cancer types. (3) Tissue Architecture Remodeling: Through enrichment in cell adhesion complexes (desmosomes, connexins) and extracellular matrix regulators, PRSS22 emerges as a facilitator of metastatic competence. Its proteolytic activity may directly cleave junctional proteins (e.g., cadherins) or activate metalloproteinases, enabling invasion through physical barrier degradation<sup>47</sup>.

The observed expression heterogeneity—overexpressed in LUAD/BLCA yet downregulated in KICH—highlights tissue-specific functional adaptation. Rather than a unitary mechanism, PRSS22 appears to operate as a contextual oncoplayer: in immunogenic tumors (e.g., SKCM), it may primarily skew immune responses; in carcinomas with epithelial origins (e.g., LIHC), it likely drives invasion through matrix remodeling. This plasticity aligns with the “cancer attractor” theory, where genes adopt tissue-specific roles within dysregulated networks<sup>48,49</sup>. Future studies could dissect these mechanisms through CRISPR screens in organoid models spanning multiple cancer types, while clinical translation efforts could explore PRSS22 as: (1) A composite biomarker integrating immune/stromal signatures; (2) A therapeutic target for protease inhibitors in selected malignancies; (3) A predictor of immunotherapy response based on its PD-1 pathway links. Collectively, PRSS22 exemplifies how multi-omics frameworks can decode functional pleiotropy in cancer, revealing how molecular players adapt their roles across tissue ecosystems to drive oncogenesis.

It should be noted that there are certain limitations: correlative findings require experimental validation of immune-pathway causality; public data heterogeneity (notably semi-quantitative HPA IHC and single-cell batch effects) constrains quantification accuracy; prognostic models demonstrate clinically modest accuracy (C-index 0.544–0.655), necessitating multi-center validation; tissue-specific mechanisms remain unresolved with therapeutic potential unconfirmed pharmacologically. Future research should prioritize experimental validation of computational findings using foundational molecular biology approaches, multi-center cohort validation, pharmacological screening, and mechanistic exploration of tissue-specific functions.

## Conclusion

In summary, our comprehensive pan-cancer multi-omics analysis identifies PRSS22 as a clinically valuable prognostic biomarker that is inherently connected to tumor-immune interactions. Its consistent abnormal expression across different cancers, links to survival outcomes, and key involvement in critical pathways—including immune regulation and microenvironment alteration—collectively highlight PRSS22 as a promising therapeutic target. Translating these findings into clinical practice could improve prognostic precision and enable personalized treatment strategies. Future research should focus on validating the immune-related functions of PRSS22 and developing targeted therapies through dedicated drug development efforts.

## Data availability

All data generated or analyzed during this study are included in this published article or supplementary information files.

Received: 27 March 2025; Accepted: 22 October 2025

Published online: 24 November 2025

## References

- Bray, F. et al. Global cancer statistics 2022: GLOBOCAN estimates of incidence and mortality worldwide for 36 cancers in 185 countries. *CA Cancer J Clin* **74**, 229–263. <https://doi.org/10.3322/caac.21834> (2024).
- Martin, C. E. & List, K. Cell surface-anchored serine proteases in cancer progression and metastasis. *Cancer Metastasis Rev.* **38**, 357–387. <https://doi.org/10.1007/s10555-019-09811-7> (2019).
- Tagirasa, R. & Yoo, E. Role of serine proteases at the tumor-stroma interface. *Front. Immunol.* **13**, 832418. <https://doi.org/10.3389/fimmu.2022.832418> (2022).
- Yasuda, S. et al. Urokinase-type plasminogen activator is a preferred substrate of the human epithelium serine protease tryptase epsilon/PRSS22. *Blood* **105**, 3893–3901. <https://doi.org/10.1182/blood-2003-10-3501> (2005).
- Wong, G. W. et al. Human tryptase epsilon (PRSS22), a new member of the chromosome 16p13.3 family of human serine proteases expressed in airway epithelial cells. *J. Biol. Chem.* **276**, 49169–49182. <https://doi.org/10.1074/jbc.M108677200> (2001).
- Song, L. et al. E2F1-initiated transcription of PRSS22 promotes breast cancer metastasis by cleaving ANXA1 and activating FPR2/ERK signaling pathway. *Cell Death Dis.* **13**, 982. <https://doi.org/10.1038/s41419-022-05414-3> (2022).
- Shi, X. et al. Building a translational cancer dependency map for The Cancer Genome Atlas. *Nat. Cancer* **5**, 1176–1194. <https://doi.org/10.1038/s43018-024-00789-y> (2024).
- Uhlen, M. et al. Proteomics. Tissue-based map of the human proteome. *Science* **347**, 1260419. <https://doi.org/10.1126/science.1260419> (2015).
- Xu, C. et al. Single-cell transcriptomics in colorectal cancer uncover the potential of metastasis and immune dysregulation of a cell cluster overexpressed PRSS22. *Front. Immunol.* **16**, 1586428. <https://doi.org/10.3389/fimmu.2025.1586428> (2025).
- Karlsson, M. et al. A single-cell type transcriptomics map of human tissues. *Sci. Adv.* **7**, eabh2169. <https://doi.org/10.1126/sciadv.aah2169> (2021).
- Vivian, J. et al. Toil enables reproducible, open source, big biomedical data analyses. *Nat. Biotechnol.* **35**, 314–316. <https://doi.org/10.1038/nbt.3772> (2017).
- Tang, Z., Kang, B., Li, C., Chen, T. & Zhang, Z. GEPIA2: An enhanced web server for large-scale expression profiling and interactive analysis. *Nucleic Acids Res.* **47**, W556–W560. <https://doi.org/10.1093/nar/gkz430> (2019).
- Jumper, J. et al. Highly accurate protein structure prediction with AlphaFold. *Nature* **596**, 583–589. <https://doi.org/10.1038/s41586-021-03819-2> (2021).

14. Liu, J. et al. An integrated TCGA pan-cancer clinical data resource to drive high-quality survival outcome analytics. *Cell* **173**, 400–416 e411. <https://doi.org/10.1016/j.cell.2018.02.052> (2018).
15. Han, Y. et al. TISCH2: expanded datasets and new tools for single-cell transcriptome analyses of the tumor microenvironment. *Nucleic Acids Res.* **51**, D1425–D1431. <https://doi.org/10.1093/nar/gkac959> (2023).
16. Szklarczyk, D. et al. The STRING database in 2025: Protein networks with directionality of regulation. *Nucleic Acids Res.* **53**, D730–D737. <https://doi.org/10.1093/nar/gkae1113> (2025).
17. Li, T. et al. TIMER2.0 for analysis of tumor-infiltrating immune cells. *Nucleic Acids Res.* **48**, W509–W514. <https://doi.org/10.1093/nar/gkaa407> (2020).
18. Newman, A. M. et al. Robust enumeration of cell subsets from tissue expression profiles. *Nat. Methods* **12**, 453–457. <https://doi.org/10.1038/nmeth.3337> (2015).
19. Chen, B., Khodadoust, M. S., Liu, C. L., Newman, A. M. & Alizadeh, A. A. Profiling tumor infiltrating immune cells with CIBERSORT. *Methods Mol. Biol.* **1711**, 243–259. [https://doi.org/10.1007/978-1-4939-7493-1\\_12](https://doi.org/10.1007/978-1-4939-7493-1_12) (2018).
20. Bindea, G. et al. Spatiotemporal dynamics of intratumoral immune cells reveal the immune landscape in human cancer. *Immunity* **39**, 782–795. <https://doi.org/10.1016/j.immuni.2013.10.003> (2013).
21. Tietscher, S. et al. A comprehensive single-cell map of T cell exhaustion-associated immune environments in human breast cancer. *Nat. Commun.* **14**, 98. <https://doi.org/10.1038/s41467-022-35238-w> (2023).
22. Kanehisa, M. & Goto, S. KEGG: Kyoto encyclopedia of genes and genomes. *Nucleic Acids Res.* **28**, 27–30. <https://doi.org/10.1093/nar/28.1.27> (2000).
23. Kanehisa, M., Sato, Y., Kawashima, M., Furumichi, M. & Tanabe, M. KEGG as a reference resource for gene and protein annotation. *Nucleic Acids Res.* **44**, D457–462. <https://doi.org/10.1093/nar/gkv1070> (2016).
24. Kanehisa, M., Furumichi, M., Sato, Y., Matsuura, Y. & Ishiguro-Watanabe, M. KEGG: Biological systems database as a model of the real world. *Nucleic Acids Res.* **53**, D672–D677. <https://doi.org/10.1093/nar/gkae909> (2025).
25. Xu, S. et al. Using clusterProfiler to characterize multiomics data. *Nat. Protoc.* **19**, 3292–3320. <https://doi.org/10.1038/s41596-024-01020-z> (2024).
26. Subramanian, A. et al. Gene set enrichment analysis: A knowledge-based approach for interpreting genome-wide expression profiles. *Proc. Natl. Acad. Sci. U S A* **102**, 15545–15550. <https://doi.org/10.1073/pnas.0506580102> (2005).
27. de Bruijn, I. et al. Analysis and visualization of longitudinal genomic and clinical data from the AACR project GENIE biopharma collaborative in cBioPortal. *Cancer Res.* **83**, 3861–3867. <https://doi.org/10.1158/0008-5472.CAN-23-0816> (2023).
28. Pawar, N. R., Buzza, M. S. & Antalis, T. M. Membrane-anchored serine proteases and protease-activated receptor-2-mediated signaling: Co-conspirators in cancer progression. *Cancer Res.* **79**, 301–310. <https://doi.org/10.1158/0008-5472.CAN-18-1745> (2019).
29. Wenta, T., Nastaly, P., Lipinska, B. & Manninen, A. Remodeling of the extracellular matrix by serine proteases as a prerequisite for cancer initiation and progression. *Matrix Biol.* **134**, 197–219. <https://doi.org/10.1016/j.matbio.2024.10.007> (2024).
30. Soman, A. & Asha Nair, S. Unfolding the cascade of SERPINA3: Inflammation to cancer. *Biochim. Biophys. Acta Rev. Cancer* **1877**, 188760. <https://doi.org/10.1016/j.bbcan.2022.188760> (2022).
31. Malhotra, Y. et al. Advancements in protein structure prediction: A comparative overview of AlphaFold and its derivatives. *Comput. Biol. Med.* **188**, 109842. <https://doi.org/10.1016/j.combiomed.2025.109842> (2025).
32. Otasek, D., Morris, J. H., Boucas, J., Pico, A. R. & Demchak, B. Cytoscape automation: Empowering workflow-based network analysis. *Genome Biol.* **20**, 185. <https://doi.org/10.1186/s13059-019-1758-4> (2019).
33. Kataoka, H., Kawaguchi, M., Fukushima, T. & Shimomura, T. Hepatocyte growth factor activator inhibitors (HAI-1 and HAI-2): Emerging key players in epithelial integrity and cancer. *Pathol. Int.* **68**, 145–158. <https://doi.org/10.1111/pin.12647> (2018).
34. Chu, Y. et al. Pan-cancer T cell atlas links a cellular stress response state to immunotherapy resistance. *Nat. Med.* **29**, 1550–1562. <https://doi.org/10.1038/s41591-023-02371-y> (2023).
35. Zheng, L. et al. Pan-cancer single-cell landscape of tumor-infiltrating T cells. *Science* **374**, abe6474. <https://doi.org/10.1126/science.abe6474> (2021).
36. Jiang, Y., Han, Q., Zhao, H. & Zhang, J. Promotion of epithelial-mesenchymal transformation by hepatocellular carcinoma-educated macrophages through Wnt2b/beta-catenin/c-Myc signaling and reprogramming glycolysis. *J. Exp. Clin. Cancer Res.* **40**, 13. <https://doi.org/10.1186/s13046-020-01808-3> (2021).
37. Charoentong, P. et al. Pan-cancer immunogenomic analyses reveal genotype-immunophenotype relationships and predictors of response to checkpoint blockade. *Cell Rep.* **18**, 248–262. <https://doi.org/10.1016/j.celrep.2016.12.019> (2017).
38. Philip, M. et al. Chromatin states define tumour-specific T cell dysfunction and reprogramming. *Nature* **545**, 452–456. <https://doi.org/10.1038/nature22367> (2017).
39. Pichler, A. C. et al. TCR-independent CD137 (4-1BB) signaling promotes CD8(+)-exhausted T cell proliferation and terminal differentiation. *Immunity* **56**, 1631–1648 e1610. <https://doi.org/10.1016/j.immuni.2023.06.007> (2023).
40. Sleebloom, J. J. F. et al. The extracellular matrix as hallmark of cancer and metastasis: From biomechanics to therapeutic targets. *Sci. Transl. Med.* **16**, eadg3840. <https://doi.org/10.1126/scitranslmed.adg3840> (2024).
41. Lavoie, H., Gagnon, J. & Therrien, M. ERK signalling: A master regulator of cell behaviour, life and fate. *Nat. Rev. Mol. Cell Biol.* **21**, 607–632. <https://doi.org/10.1038/s41580-020-0255-7> (2020).
42. Ping, Y. et al. PD-1 signaling limits expression of phospholipid phosphatase 1 and promotes intratumoral CD8(+) T cell ferroptosis. *Immunity* **57**, 2122–2139 e2129. <https://doi.org/10.1016/j.immuni.2024.08.003> (2024).
43. He, Y. et al. Targeting PI3K/Akt signal transduction for cancer therapy. *Signal Transduct. Target Ther.* **6**, 425. <https://doi.org/10.1038/s41392-021-00828-5> (2021).
44. Ghosh, M. et al. Mutant p53 suppresses innate immune signaling to promote tumorigenesis. *Cancer Cell* **39**, 494–508 e495. <https://doi.org/10.1016/j.ccell.2021.01.003> (2021).
45. Shoshani, O. et al. Chromothripsis drives the evolution of gene amplification in cancer. *Nature* **591**, 137–141. <https://doi.org/10.1038/s41586-020-03064-z> (2021).
46. van der Leun, A. M., Thommen, D. S. & Schumacher, T. N. CD8(+) T cell states in human cancer: Insights from single-cell analysis. *Nat. Rev. Cancer* **20**, 218–232. <https://doi.org/10.1038/s41568-019-0235-4> (2020).
47. Pawar, N. R., Buzza, M. S., Duru, N., Strong, A. A. & Antalis, T. M. Matriptase drives dissemination of ovarian cancer spheroids by a PAR-2/PI3K/Akt/MMP9 signaling axis. *J. Cell Biol.* **222**, e202209114. <https://doi.org/10.1083/jcb.202209114> (2023).
48. Huang, S. Reconciling non-genetic plasticity with somatic evolution in cancer. *Trends Cancer* **7**, 309–322. <https://doi.org/10.1016/j.trecan.2020.12.007> (2021).
49. Huang, S., Ernberg, I. & Kauffman, S. Cancer attractors: A systems view of tumors from a gene network dynamics and developmental perspective. *Semin. Cell Dev. Biol.* **20**, 869–876. <https://doi.org/10.1016/j.semcdb.2009.07.003> (2009).

## Acknowledgements

We are grateful to all the participants who contributed to this study. Special thanks go to the Xiantao Academic Platform ([www.xiantao.love](http://www.xiantao.love)) for its technical support in data processing and analysis.

## Author contributions

Tao Jiang wrote the main manuscript text. Jialin Liu, Hao Chen, and Fangyu Lin were responsible for data analysis. Xiaojiao Weng, Qing Liu, and Han Wang prepared Figs. 1–3. Bin Du and Xinli Wang prepared Figs. 4–6 and figures S1–2. Xiaoyan Lin and Wenyu Gao were responsible for the article review.

## Funding

This study was supported by the National Natural Science Foundation of China (NSFC), Young Scientists Fund (Grant Number: 82203777), Fujian Provincial Natural Science Foundation of China (Grant Number: 2021J01736), and Joint Funds for the Innovation of Science and Technology, Fujian province (Grant Number: 2021Y9045).

## Declarations

### Competing interests

The authors declare no competing interests.

### Disclosures

Tao Jiang, Jialin Liu, Hao Chen, Fangyu Lin, Xiaojiao Weng, Qing Liu, Han Wang, Bin Du, Xinli Wang, Xiaoyan Lin, Wenyu Gao have nothing to disclose.

### Additional information

**Supplementary Information** The online version contains supplementary material available at <https://doi.org/10.1038/s41598-025-25604-1>.

**Correspondence** and requests for materials should be addressed to W.G.

**Reprints and permissions information** is available at [www.nature.com/reprints](http://www.nature.com/reprints).

**Publisher's note** Springer Nature remains neutral with regard to jurisdictional claims in published maps and institutional affiliations.

**Open Access** This article is licensed under a Creative Commons Attribution-NonCommercial-NoDerivatives 4.0 International License, which permits any non-commercial use, sharing, distribution and reproduction in any medium or format, as long as you give appropriate credit to the original author(s) and the source, provide a link to the Creative Commons licence, and indicate if you modified the licensed material. You do not have permission under this licence to share adapted material derived from this article or parts of it. The images or other third party material in this article are included in the article's Creative Commons licence, unless indicated otherwise in a credit line to the material. If material is not included in the article's Creative Commons licence and your intended use is not permitted by statutory regulation or exceeds the permitted use, you will need to obtain permission directly from the copyright holder. To view a copy of this licence, visit <http://creativecommons.org/licenses/by-nc-nd/4.0/>.

© The Author(s) 2025